PUSHBELT CVTS - A NON-SMOOTH CHALLENGE

Thorsten Schindler
Institute of Applied Mechanics
Technische Universität München
D-85747 Garching, Germany
schindler@amm.mw.tum.de
Tel./Fax: +498928915-216/213

Heinz Ulbrich
Institute of Applied Mechanics
Technische Universität München
D-85747 Garching, Germany
ulbrich@amm.mw.tum.de
Tel./Fax: +498928915-222/213

Friedrich Pfeiffer
Institute of Applied Mechanics
Technische Universität München
D-85747 Garching, Germany
pfeiffer@amm.mw.tum.de
Tel./Fax: +498928915-200/213

Arie van der Velde
CVT Advanced Engineering
Van Doorne's Transmissie b.v. / Bosch Group
NL-5026 RA Tilburg, Netherlands
Arie.vanderVelde@nl.bosch.com
Tel./Fax: +311346-40353/36590

Arjen Brandsma
CVT Advanced Engineering
Van Doorne's Transmissie b.v. / Bosch Group
NL-5026 RA Tilburg, Netherlands
Arjen.Brandsma@nl.bosch.com
Tel./Fax: +311346-40441/36590

Abstract
This paper deals with a spatial transient mathematical model of pushbelt Continuously Variable Transmissions (CVT) characterised by numerous contacts and a large degree of freedom. The non-smooth equations of motion are derived using methods of multibody theory and nonlinear mechanics. Thereby, the bodies themselves are described using rigid and large deflection elastic mechanical models. In-between the bodies, all possible flexible or rigid contact descriptions, namely frictionless unilateral contacts, bilateral contacts with 2D-friction and even unilateral contacts with 3D-friction occur. The resulting stiff measure differential inclusion (MDI) is integrated using robust and efficient time-stepping schemes.

Key words
non-smooth dynamics, flexible multibody system, computational mechanics, time-stepping scheme, continuously variable transmission

1 Introduction

In contrast to smooth mechanical systems, acceleration and even velocity jumps can occur in non-smooth systems normally induced by impacts and rigid contacts. Although these velocity jumps could be avoided by using regularised contact models, it is numerically better to integrate the non-smooth equations. Then, a solution can be calculated more efficiently and stable avoiding a high numerical stiffness due to springs. Since the 1980s, the theory and numerics of non-smooth mechanics has been a major research area for the Institute of Applied Mechanics of the Technische Universität München. Especially with the mathematical formulation of PFEIFFER and GLOCKER (Pfeiffer and Glocker, 1996; Glocker, 2001), the time-stepping schemes of STIEGELMEYR and FUNK (Stiegelmeyr, 2001; Funk, 2004) and the further developments of FÖRG (Förg, 2007) mainly with respect to the evaluation of set-valued force laws, it is possible to integrate even complex industrial systems, for example pushbelt CVTs.

A pushbelt CVT is an alternative transmission system with high expectations. Especially the optimal operation of the whole drive train including the engine explains the increasing production volume of this transmission type. Per year about three million pushbelts are installed in over 70 different vehicle models.

In an ongoing cooperation with Bosch, a mathematical model for the planar dynamics of the pushbelt CVT was established and validated (Geier, 2007). It is compared with measurement data close to normal operating conditions (Schindler *et al.*, 2007) and shows, how a profound understanding of the dynamics can be achieved without mostly expensive and elaborate experiments. But further, the model can be used to identify the potential of the pushbelt CVT with respect to industrially relevant topics like fuel consumption. This supported the improvement in the emissions' properties by a new "slip control" strategy investigated by Bosch (van der Sluis *et al.*, 2006).

With a spatial model of the pushbelt CVT it would be possible to consider even out-of plane effects for instance pushbelt misalignment. So in time of tightening emission legislation, further optimisations could be investigated concerning comfort, cost, fun to drive and especially fuel consumption.

2 Non-Smooth Multibody Systems

The theory of the dynamics of systems with constraints, friction and frictional impacts can be expressed in the sense of distributions or by a measure differential equation

$$\boldsymbol{M}\boldsymbol{\mu}^{\boldsymbol{u}} = \boldsymbol{\mu}^{\boldsymbol{G}} + \sum_k \boldsymbol{\mu}^{\boldsymbol{H}_k} \tag{1}$$

together with complementarity equations. Thereby, the measures $\boldsymbol{\mu}$ represent the velocity by the superscript $\boldsymbol{u}$, LEBESGUE-integrable forces by $\boldsymbol{G}$ and impacts at time t_k by the Heaviside functions $\boldsymbol{H}_k$. The symmetric and positive definite mass matrix $\boldsymbol{M}$ depends on the position $\boldsymbol{q}$ of the system.

It is also possible to distinguish between smooth and impact dynamics. Then, the equations of motion can be written like

$$\boldsymbol{M}\dot{\boldsymbol{u}} = \boldsymbol{h} + \boldsymbol{W}\boldsymbol{\lambda}\,, \tag{2}$$

$$\boldsymbol{M}_k\left(\boldsymbol{u}_k^+ - \boldsymbol{u}_k^-\right) = \boldsymbol{W}_k\boldsymbol{\Lambda}_k \quad \forall k \tag{3}$$

using $\dot{\boldsymbol{u}}$ for denoting the weak time derivative of $\boldsymbol{u}$ and $\boldsymbol{u}_k^+$ as well as $\boldsymbol{u}_k^-$ for describing the velocity after and before an impact time. The vector $\boldsymbol{h}$ contains all smooth forces not depending on additional constraints symbolizing rigid interactions between bodies. It is a function of $\boldsymbol{q}$, $\boldsymbol{u}$ and explicitly of t. The directions of generalised contact reactions are summarised in the matrix $\boldsymbol{W}$ as well as $\boldsymbol{\lambda}$ and $\boldsymbol{\Lambda}_k$ refer to smooth and non-smooth contact reaction values, respectively.

The complementarity equations result from the contact reaction laws defining the relationship of the contact reactions to the state $\left(\boldsymbol{q}^T, \boldsymbol{u}^T\right)^T$ of the system at the time t. Three main types of contact reaction laws can be distinguished. Considering only smooth motion, on position level they are given by a bilateral constraint

$$g_N = 0, \quad \lambda_N \lessgtr 0 \tag{4}$$

and an unilateral constraint

$$\lambda_N \geq 0, \quad g_N \geq 0, \quad \lambda_N g_N = 0 \tag{5}$$

for the normal contact distance g_N. COULOMB dry friction for the tangential contact gaps $\boldsymbol{g}_T$ is represented by

$$\|\boldsymbol{\lambda}_T\| \leq \mu\lambda_N \quad \text{for} \quad \dot{\boldsymbol{g}}_T = \boldsymbol{0}\,, \tag{6}$$

$$\boldsymbol{\lambda}_T = -\mu\lambda_N \frac{\dot{\boldsymbol{g}}_T}{\|\dot{\boldsymbol{g}}_T\|} \quad \text{for} \quad \dot{\boldsymbol{g}}_T \neq \boldsymbol{0}\,, \tag{7}$$

if the normal distance g_N is zero. The constant friction coefficient is denoted by μ.

An impact influences all contacts between bodies concerning the post impact velocity. So, the impact laws have to be formulated on velocity level substituting g by $\dot{g}^+$ and λ by Λ in the complementarity equations subject to the condition, that the affected contact is closed. In this context, it is even possible to define special impact laws by replacing $\dot{g}^+$ with adequate physical approximations to regard for example elastic impact behaviour.

With the description outlined above, a mechanical system is divided in the motion of bodies and in the interaction between bodies. Only missing is the calculation of the direction matrix of generalised contact reactions $\boldsymbol{W}$, the gaps g and relative velocities $\dot{g}$. This is done by assigning a contour to a body in general characterised by a 2D-contour parameter vector $\boldsymbol{s}$. Then assuming unique point-to-point contacts, the contact parameters $\boldsymbol{s}_{c_1}$ and $\boldsymbol{s}_{c_2}$ for two contacting bodies necessarily fulfill

$$\boldsymbol{T}_1^T\left(\boldsymbol{s}_{c_1}\right)\left[\boldsymbol{r}_1\left(\boldsymbol{s}_{c_1}\right) - \boldsymbol{r}_2\left(\boldsymbol{s}_{c_2}\right)\right] = \boldsymbol{0}\,, \tag{8}$$

$$\boldsymbol{T}_2^T\left(\boldsymbol{s}_{c_2}\right)\left[\boldsymbol{r}_1\left(\boldsymbol{s}_{c_1}\right) - \boldsymbol{r}_2\left(\boldsymbol{s}_{c_2}\right)\right] = \boldsymbol{0} \tag{9}$$

with the inertial position $\boldsymbol{r}$ of the bodies and the tangent matrix $\boldsymbol{T} = \frac{\partial \boldsymbol{r}}{\partial \boldsymbol{s}}$. Depending on the structure of these equations either analytical or numerical methods have to be applied to get a set of potential contact parameters. Selecting the solution with minimal distance

$$g_N = \boldsymbol{n}_1^T\left(\boldsymbol{s}_{c_1}\right)\left[\boldsymbol{r}_1\left(\boldsymbol{s}_{c_1}\right) - \boldsymbol{r}_2\left(\boldsymbol{s}_{c_2}\right)\right] \tag{10}$$

allows calculating the relative normal and tangential velocities by projection of the relative velocity on the corresponding matrices $\boldsymbol{n}$ and $\boldsymbol{T}$. The matrix $\boldsymbol{W}$ is the projection of the Cartesian directions $\boldsymbol{n}$ and $\boldsymbol{T}$ of contact reactions in the space of generalised velocities $\boldsymbol{u}$ by appropriate JACOBIAN matrices.

3 Numerical Treatment

In contrast to event-driven schemes so-called time-stepping schemes can handle even a large number of contact transitions describing the time-variant topology of non-smooth systems. They are based on the discretisation of the equations of motion including the complementarity equations not adapting the globally fixed time step size Δt due to closing contacts. This forces the integrator to be very sensible with respect to the time step size, numerical stability and accuracy; on the other hand it allows to focus on the global physical behaviour of the simulated models minimising the number of combinatorial problems and therefore increasing computational efficiency (Stiegelmeyr, 2001; Leine and Glocker, 2003; Funk, 2004; Förg, 2007).

In this paper a half-explicit time-stepping algorithm of order one is used, whereby a single integration step $l \rightarrow l+1$ can be summarised as follows:

1. Update the positions $\boldsymbol{q}^{l+1} = \boldsymbol{q}^l + \boldsymbol{u}^l\Delta t$.

2. Compute the velocities considering violated constraints on velocity level labeled by subscript v

$$\boldsymbol{M}^{l+1}\Delta\boldsymbol{u}^{l} = \hat{\boldsymbol{h}}^{\,l+1}\,\Delta t + \boldsymbol{W}_{v}^{l+1}\,\boldsymbol{\Lambda}_{v}^{l+1}\,, \quad \text{(11a)}$$

$$\dot{\boldsymbol{g}}_{v}^{l+1} = \dot{\boldsymbol{g}}_{v}(\boldsymbol{u}^{l+1}, \boldsymbol{q}^{l+1}, t^{l+1})\,, \quad \text{(11b)}$$

$$\boldsymbol{\Lambda}_{v}^{l+1} = \mathbf{proj}(\dot{\boldsymbol{g}}_{v}^{l+1}, \boldsymbol{\Lambda}_{v}^{l+1})\,. \quad \text{(11c)}$$

The evaluation $\hat{\boldsymbol{h}}^{\,l+1} = \boldsymbol{h}(\boldsymbol{u}^{l}, \boldsymbol{q}^{l+1}, t^{l+1})$ is half-explicit and increases the numerical stability. An augmented LAGRANGIAN formulation of the complementarity equations is denoted by **proj** using the theory of proximal points (Alart and Curnier, 1991) as well as numerical acceleration and stabilizing methods (Förg, 2007).

3. Correct numerical drifts.

4 Modelling of Pushbelt CVTs

An input and an output pulley as well as the pushbelt set up the variator of the transmission system (left side of Figure 1). Thereby, each of the pulleys consists

Figure 1. Pushbelt variator and pushbelt with elements

of a fixed and an axially moveable V-shaped sheave. The pushbelt is composed of approximately 400 elements, which are guided by two ring packages of nine to twelve steel rings (right hand side of Figure 1). Figure 2 shows the functionality for two different transmission ratios. Here, $\dot{\gamma}$ denotes the angular velocity of a pulley, M the torque and F_C the clamping force acting on the loose sheave. The torque is transmitted from the input to the output pulley via friction forces between the pushbelt and the sheaves and further on via push and tension forces within the pushbelt. By applying hydraulic pressures on the loose sheaves, their axial positions can be changed, modifying the effective running radii of the pushbelt within the pulleys continuously.

The model is established in two steps yielding the general equations of section 2:

1. The decoupled motion of pulleys, elements and ring packages is described.
2. The interactions between these bodies as well as the environment are accounted for.

For the whole variator model the following points have to kept in mind:

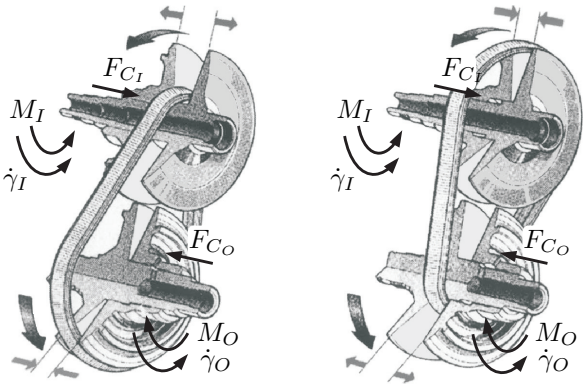

Figure 2. Functionality of the pushbelt variator

1. The inertial frame of reference (FR) of the whole CVT is located in the centre of the output pulley symmetric between the input and output fixed sheave; the $\boldsymbol{x}_I$-axis is in direction to the input pulley and the $\boldsymbol{z}_I$-axis in axial direction to the output fixed sheave. The $\boldsymbol{y}_I$-axis axis develops a positive Cartesian coordinate system.
2. Elasticities of pulleys and elements can be considered within the interaction quasistatically, because such deformations only happen in case of contact and effect in a much smaller scale than global motions.
3. The equations are only shown for smooth dynamics; the impact equations can be derived analogously.
4. Gravity is considered for all components.

4.1 Ring Package

Homogenising the layered structure, the two ring packages are modelled by a 1D continuum divided in a number N_b of FE-beams. As a transient model of the CVT is desired, no reference path of the ring package can be given. So, the model has to describe free motion with geometrically nonlinear, large deformations, but linear material laws. According to a redundant coordinate method (RCM) of ROLAND ZANDER and HEINZ ULBRICH (Zander and Ulbrich, 2006*b*; Zander and Ulbrich, 2006*a*) comparatively efficiently describing the planar motion of large deformation beams, an extension has been derived for the 3D ring packages. It gives an accurate, comprehensive approach based on the physically interpretable ideas of EULER-BERNOULLI beam formulations. Thereby, the advantages of both moving frame of reference (MFR) and finite element (FE) concepts can be maintained:
Each FE-beam is defined with respect to an inertial FR of the ring package. Representing 3D angle parametrisation of accompanying trihedrals ($\boldsymbol{t}$, $\boldsymbol{n}$, $\boldsymbol{b}$) and ring structures in the plane of motion of the CVT, the FR of the ring package is located in the origin of the inertial FR with an adequate rotational transformation.
For the derivation of compact equations of motions, a so-called internal coordinate set (Figure 3)

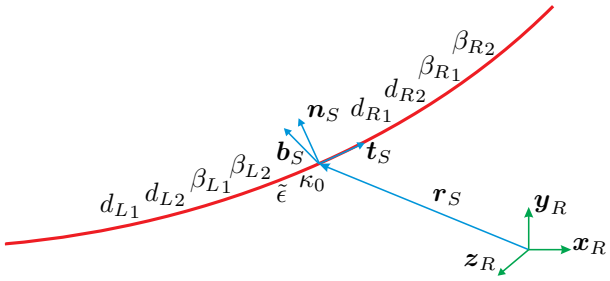

Figure 3. Internal coordinates

$$\boldsymbol{q}_{\mathrm{i}} := (x_S, y_S, z_S, \varphi_{S0}, \varphi_{S1}, \varphi_{S2}, \tilde{\epsilon}, d_{L1}, d_{R1}, \beta_{L1}, \beta_{R1}, d_{L2}, d_{R2}, \beta_{L2}, \beta_{R2}, \kappa_0)^T \quad (12)$$

is used separating rigid ($\boldsymbol{r}_S^T = (x_S, y_S, z_S)$, φ_{S0}, φ_{S1}, φ_{S2}) and elastic body motion including elongation ($\tilde{\epsilon}$), bending (d_{L1}, d_{R1}, β_{L1}, β_{R1}, d_{L2}, d_{R2}, β_{L2}, β_{R2}) and torsion (κ_0). It parametrises the neutral fibre representing a mixture of co-rotational and inertial frame approaches. Based on expressions for the elastic, kinetic and gravitational energy, the equations of motion of the FE-beams themselves are calculated with the LAGRANGE II formalism. Extending the result with damping yields the equations of motion in terms of the internal coordinates

$$\boldsymbol{M}_{\mathrm{i}}\dot{\boldsymbol{u}}_{\mathrm{i}} - \boldsymbol{h}_{\mathrm{i}} = \boldsymbol{0} \quad (13)$$

with $\boldsymbol{u}_{\mathrm{i}} = \dot{\boldsymbol{q}}_{\mathrm{i}}$. A second coordinate set (Figure 4) shifts

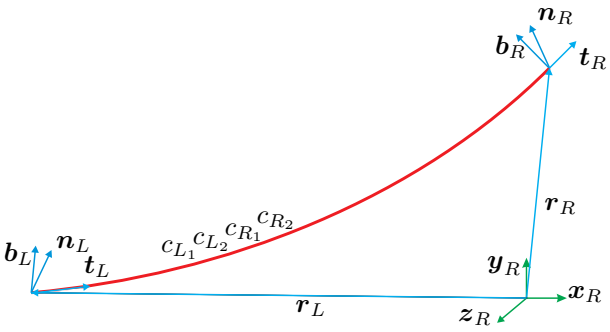

Figure 4. Global coordinates

the main information of the FE-beams to their left and right end points:

$$\boldsymbol{q}_{\mathrm{g}} := (x_L, y_L, z_L, \varphi_{L0}, \varphi_{L1}, \varphi_{L2}, c_{L_1}, c_{R_1}, c_{L_2}, c_{R_2}, x_R, y_R, z_R, \varphi_{R0}, \varphi_{R1}, \varphi_{R2})^T . \quad (14)$$

Thereby, c_{L_1}, c_{R_1}, c_{L_2} and c_{R_2} symbolise interior bending deflections. After having defined a transformation between the two coordinate sets, the assembling in global coordinates does not invoke any additional constraints. This yields the sparse equations of motion of a ring package with k FE-beams

$$\sum_{j=1}^{k} \boldsymbol{J}_{\mathrm{i_j r}}^T \left[\boldsymbol{M}_{\mathrm{i_j}} \boldsymbol{J}_{\mathrm{i}_j r} \dot{\boldsymbol{u}}_{\mathrm{r}} - \boldsymbol{h}_{\mathrm{i_j}} - \boldsymbol{M}_{\mathrm{i_j}} \dot{\boldsymbol{J}}_{\mathrm{i_j r}} \boldsymbol{u}_{\mathrm{r}} \right] = \boldsymbol{0} \quad (15)$$

projected in the space of the minimal velocity coordinates $\boldsymbol{u}_{\mathrm{r}}$ by the JACOBIAN matrices $\boldsymbol{J}_{\mathrm{i}_j \mathrm{r}} = \frac{\partial \boldsymbol{q}_{\mathrm{i_j}}}{\partial \boldsymbol{q}_{\mathrm{r}}}$. The equations can be implemented very efficiently by index-scanning for used degrees of freedom. Then, operations on non-zero entries can be avoided.

4.2 Elements

Altogether, N_e rigid elements with $\mathrm{dof} = 6$, respectively, will be used for the CVT dynamics representing 3D angle parametrisation. Figure 5 depicts the element shape schematically. Thereby, the local FR is located

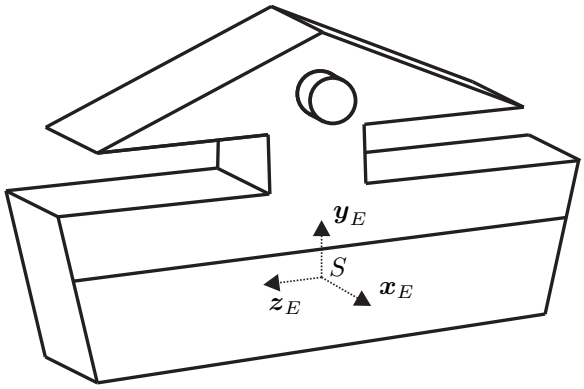

Figure 5. Element - 3D Perspective

in the Centre of Gravity (COG) S. The $\boldsymbol{x}_E$-axis is perpendicular to the planar rear side of each element and in direction to the front side, whereas the $\boldsymbol{y}_E$-axis is perpendicular to the planar bottom of each element in direction to the top. The $\boldsymbol{z}_E$-axis completes the $\boldsymbol{x}_E$- and $\boldsymbol{y}_E$-axis to a positive Cartesian coordinate system. This results in the canonical equations of motion of the elements using the NEWTON-EULER formalism.

4.3 Pulleys

As the axis of the pulleys is modelled rigidly, only the sheaves have to be discussed. The loose sheaves fulfill $\mathrm{dof} = 2$ representing translation along and rotation about their axis. With $\mathrm{dof} = 1$, fixed sheaves can only rotate. Assuming a symmetric shape, the FR is located in the COG S of the sheaves. The $\boldsymbol{z}_S$-axis is in axial direction normal to the rear side and the $\boldsymbol{y}_S$-axis is initially parallel to the $\boldsymbol{y}_I$-axis of the inertial FR. The $\boldsymbol{x}_S$-axis completes a positive Cartesian coordinate system. Then, the equations of motion of the pulleys are canonically structured.

4.4 Interactions

For example external borders, connections and contacts are included within interactions. Thereby, a connection combines two bodies bilaterally at a relatively fixed point without defining friction. With contacts even friction can be set and moveable points of reference are possible. Contacts are always described by sets of points, whereby the intersection must consist of at most one point. For efficiency, the number of contacts is minimised.

4.4.1 Sheave-Sheave The interface between a fixed and a loose sheave is defined by a connection ensuring the same angular velocity of the sheaves. Its inertia can be considered within the sheaves.

4.4.2 Pulley-Environment There are two possibilities for the border to the environment: a kinetic and a kinematic excitation. For the output pulley only a kinetic excitation is provided. It is given by a 2D load $\boldsymbol{L}_O$ representing the clamping force F_{C_0} and the load torque M_O.
For the input pulley the rotational setting is always done by the angular velocity $\dot{\gamma}_I$. The clamping could be either a kinematic or a kinetic excitation. As the position is given by initialisation, in the first case the clamping velocity $\dot{z}_{C_I}$ is provided. In the second case the clamping force F_{C_I} is defined.

4.4.3 Element-Pulley The shape of the left and right body side of the elements is described by its extremal points, respectively. The sheaves have frustum contour. So, the contact points are uniquely given and the contact geometry allows for 3D motion of the elements, even clamping between the sheaves and friction torques. The contact reaction law is unilateral with 3D COULOMB-friction.
As a frustum is a primitive contour, it is possible to simplify the general contact solution algorithm. The contact between a point Q and a frustum with the normed axis $\boldsymbol{a}$, the radii r_1 and r_2 in direction to the axis, the height h and a starting point P at the centre of the bottom could be declared as follows. Defining

$$\varphi := \operatorname{atan}\left(\frac{r_2 - r_1}{h}\right) , \tag{16}$$

$$\boldsymbol{d} := \boldsymbol{Q} - \boldsymbol{P} , \tag{17}$$

$$r_h := r_1 + \frac{r_2 - r_1}{h} s , \tag{18}$$

$$s := \boldsymbol{a}^T \boldsymbol{d} , \tag{19}$$

$$\boldsymbol{b} := \frac{\boldsymbol{d} - s\boldsymbol{a}}{\|\boldsymbol{d} - s\boldsymbol{a}\|} \tag{20}$$

with respect to Figure 6 it can be proved, if there is contact possible by comparing $\|\boldsymbol{d} - s\boldsymbol{a}\|$ and r_h. Then,

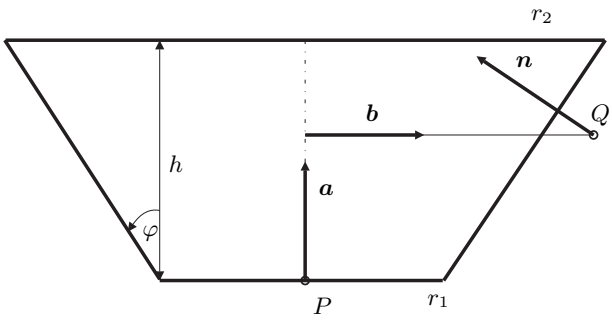

Figure 6. Frustum

the inward pointing normal can be calculated by

$$\boldsymbol{n} = \sin(\varphi)\,\boldsymbol{a} - \cos(\varphi)\,\boldsymbol{b} \tag{21}$$

and the gap is given by

$$g_N = [\|\boldsymbol{d} - s\boldsymbol{a}\| - r_h]\cos(\varphi) \ . \tag{22}$$

So, no explicit evaluation of root functions is necessary. A basis of the tangential plane can be chosen canonically and velocity depending values are calculated as described in the general procedure.

4.4.4 Element-Ring Package If one assumes only small clearance between the elements in longitudinal direction and the guidance of the elements by the ring packages avoiding detachment, this neglects a rotational interaction between the elements and the ring package. So, a minimal number of contact points at the element saddles and at the element pillar define the contact behaviour with the ring package. A bilateral contact reaction law with 2D COULOMB-friction is used for the saddle contact and a bilateral contact reaction law without friction specifies the pillar contact. Thereby, the contacting faces of the ring package are described by an appropriate adapted flexible band

$$\begin{aligned} \boldsymbol{B} : [0, l] \times \left[-\frac{b}{2}, \frac{b}{2}\right] &\to \mathbb{R}^3 , \\ (x, \mu) &\mapsto \boldsymbol{r}(x) - d_N \frac{\alpha\tilde{\boldsymbol{n}}(x) + \beta\tilde{\boldsymbol{b}}(x)}{\sqrt{\alpha^2 + \beta^2}} \\ &\quad + \mu \frac{\alpha\tilde{\boldsymbol{b}}(x) - \beta\tilde{\boldsymbol{n}}(x)}{\sqrt{\alpha^2 + \beta^2}} . \end{aligned} \tag{23}$$

It references to the neutral fibre $\boldsymbol{r}$ of the ring package with the normal $\tilde{\boldsymbol{n}}$ and binormal $\tilde{\boldsymbol{b}}$ of its parametrisation, the width b and length l of the flexible band, a normal distance d_N and the inward pointing normal direction of the flexible band $\alpha\tilde{\boldsymbol{n}} + \beta\tilde{\boldsymbol{b}}$ as linear combination.
The resulting root function of the contact problem is solved by a globalised Newton method.

4.4.5 Element-Element The dynamics between two adjacent elements can be subdivided in the interaction of extremal points at the front with a plane contour at the rear side as well as the pin-hole kinematics modelled with circle-to-frustum geometries. The contact reaction law is frictionless and unilateral.
The impact to the rear side of the neighbouring element can be reduced to a primitive description. With a point Q, the starting point P and the inward normal vector $\boldsymbol{n}$ of a general plane the formula for the gap is easy to derive and given by

$$g_N = (\boldsymbol{P} - \boldsymbol{Q})^T \boldsymbol{n} \,. \tag{24}$$

Tangential basis vectors can be chosen canonically and velocity depending values are calculated as described in the general procedure.
Even for the pin-hole contact a simplification is possible: The conic section of the circle plane and the frustum traces the contact problem back to the contact between a circle and an ellipse. The result is a scalar root function

$$\begin{aligned} 0 = {} & 2\left[-\boldsymbol{c}_1 \sin(\varphi) + \boldsymbol{c}_2 \cos(\varphi)\right]^T \left[\boldsymbol{M}_C - \boldsymbol{M}_E\right] \\ & + \sin(2\varphi)\left[\|\boldsymbol{c}_1\|^2 - \|\boldsymbol{c}_2\|^2\right] \end{aligned} \tag{25}$$

with the central points $\boldsymbol{M}_C$ and $\boldsymbol{M}_E$ of circle and ellipse as well as the semi-major and semi-minor axis vectors $\boldsymbol{c}_1$ and $\boldsymbol{c}_2$ of the ellipse. It is solved by a globalised Newton method yielding the solution parameter φ of the ellipse. This solution parameter is used to calculate the contact point on the circle. With the kinematics of a point-to-frustum contact described in section 4.4.3, it is possible to calculate the gap as well as the normal and tangents of both frustum and circle. The velocity depending values are computed as described in the general procedure.

4.5 Challenges

It is clear, that Young's modulus of the ring packages directly influences the numerical stiffness of the whole CVT and so the global time step size. But even the high contact closing frequency has to be resolved in a certain level to represent the variator dynamics. Together with the large degree of freedom of the system this causes long simulation times. Further, the initialisation results in additional instabilities, for instance because of a jump from curvature 0 in the trum to a constant curvature $\neq 0$ in the arcs not being represented exactly by the bending polynomials. To minimise the effects on the rest of the simulation, a special pre-integration has to be performed to get a physically valid, stationary state of the system.

5 Conclusion

The present paper introduces theoretical and numerical formalisms for solving non-smooth differential equations. Further, it describes the derivation of a spatial transient model of a pushbelt variator considering the components of the CVT and the different interactions separately. The resulting non-smooth differential equations are integrated by efficient time-stepping schemes. Altogether, the model can be applied to analyse the dynamics of the real system and to improve its performance concerning out-of-plane motion, misalignments, comfort and fuel consumption using mathematical optimisation methods.

References

Alart, P.; Curnier, A. (1991). A mixed formulation for frictional contact problems prone to Newton like solution methods. *Computer Methods in Applied Mechanics and Engineering* **92**, 353 – 375.

Funk, K. (2004). Simulation eindimensionaler Kontinua mit Unstetigkeiten. PhD thesis. TU München.

Förg, M. (2007). Mehrkörpersysteme mit mengenwertigen Kraftgesetzen - Theorie und Numerik. PhD thesis. TU München.

Geier, T. (2007). Dynamics of Push Belt CVTs. PhD thesis. TU München.

Glocker, C. (2001). *Set-Valued Force Laws in Rigid Body Dynamics*. Springer Verlag, Berlin.

Leine, R. I.; Glocker, C. (2003). A set-valued force law for spatial Coulomb-Contensou friction. *European Journal of Mechanics* **22**, 193–216.

Pfeiffer, F.; Glocker, C. (1996). *Multibody Dynamics with Unilateral Contacts*. John Wiley & Sons Inc., New York.

Schindler, T.; Geier, T.; Ulbrich, H.; Pfeiffer, F.; van der Velde, A.; Brandsma, A. (2007). Dynamics of Pushbelt CVTs. In: *VDI-Berichte 1997 - Umschlingungsgetriebe*. VDI-Gesellschaft Entwicklung Konstruktion Vertrieb. Berlin.

Stiegelmeyr, A. (2001). Zur numerischen Berechnung strukturvarianter Mehrkörpersysteme. PhD thesis. TU München.

van der Sluis, F.; van Dongen, T.; van Spijk, G.-J.; van der Velde, A.; van Heeswijk, A. (2006). Fuel Consumption Potential of the Pushbelt CVT. In: *FISITA 2006 World Automotive Congress*.

Zander, R.; Ulbrich, H. (2006*a*). Free plain motion of flexible beams in MBS - A comparison of models. *Journal of Mechanics Based Design of Strucures and Machines* **34**(4), 365–387.

Zander, R.; Ulbrich, H. (2006*b*). Reference-free mixed FE-MBS approach for beam structures with constraints. *Nonlinear Dynamics* **46**, 349–361.